# On the interactions between atmospheric radicals and cloud droplets: A molecular picture of the interface

**Qicun Shi, Stephen D. Belair, Joseph S. Francisco*, and Sabre Kais***

Department of Chemistry, Purdue University, West Lafayette, IN 47907

Communicated by Raphael D. Levine, Hebrew University of Jerusalem, Jerusalem, Israel, June 16, 2003 (received for review March 4, 2003)

**How gas-phase materials become incorporated with cloud droplets has been an intriguing subject for decades, and considerable work has been done to understand the interactions between closed-shell molecules and liquid water. The interactions between open-shell radical species and liquid-phase cloud droplets, however, are not well understood. To probe these interactions we used quantum chemistry calculations to predict the energetics of the hydroperoxy radical ($HO_2$) in the presence of an $(H_2O)_{20}$ spherical water cage. Our calculations show that it is energetically favorable for the radical to bind to the outside of the cage. This configuration has the hydrogen and the terminal oxygen of the radical as its primary bonding sites. Free-energy calculations suggest that, at atmospheric conditions, there will be a partitioning between $HO_2$ radicals that are surface-bound and $HO_2$ radicals that dissolve into the bulk. This may have important ramifications for our understanding of radical chemistry and may lend insight into the role that clouds and aerosols play in atmospheric chemical processes.**

Radical species play an important role in controlling the chemistry of the atmosphere. The uptake of radicals by both aqueous atmospheric aerosols and cloud droplets can impact gas-phase chemistry by removing reactant radicals from the gas phase. For example, the uptake of $HO_2$ radicals by cloud droplets slows down the gas-phase loss of ozone ($O_3$) because $HO_2$ can react with $O_3$ as follows (1):

$$HO_2 + O_3 \rightarrow OH + 2O_2.$$

Lack of $HO_2$ concentration can also suppress the formation of $O_3$ by the reaction sequence

$$HO_2 + NO \rightarrow NO_2 + OH$$

$$NO_2 + h\nu \rightarrow NO + O$$

$$O_2 + O \rightarrow O_3.$$

However, the mechanism by which $HO_2$ is taken up by an aqueous medium and what happens to the $HO_2$ after uptake both are unclear. Knowing whether a particular radical species is adsorbed (surface-bound) or absorbed (dissolved into the bulk) is critical to an understanding of its kinetics and reaction dynamics.

The current model for how a gas-phase molecule is taken up by a water droplet (2) is depicted in Fig. 1. The first step involves gas-phase diffusion to the surface of the droplet. The second step involves accommodation of the gas-phase molecule at the surface. This is the crucial step, and little is known about how a radical interacts with the surface. Studies by Gertner and Hynes (3) have looked at how closed-shell molecules interact with water surfaces, but no studies to date have explained how open-shell species might be accommodated. Once a molecule is accommodated, the third step involves diffusion within the water droplet. Reaction within the bulk, diffusion of the reaction products back to the surface, and desorption from the droplet make up the remainder of the sequence. An understanding of each of these steps is essential to comprehend reactive uptake by water droplets, which is important for atmospheric models and the interpretation of heterogeneous processes occurring in the atmosphere.

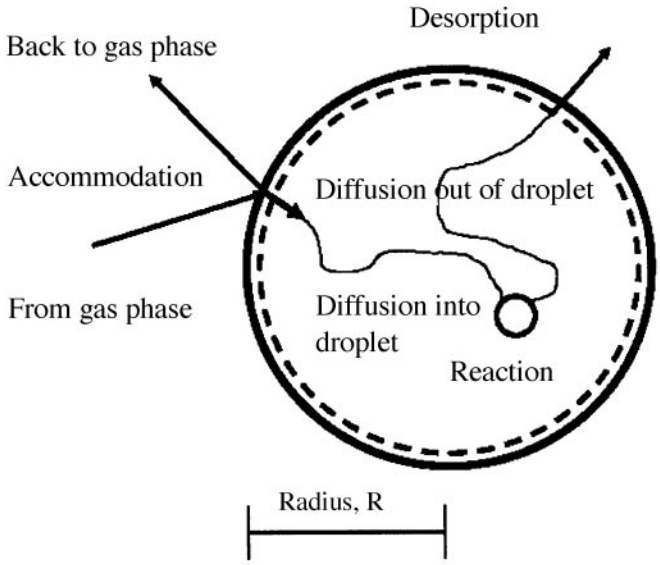


**Fig. 1.** A schematic representation of the processes involved in the reactive uptake of a radical by a cloud droplet, $R \approx 1$–$20$ $\mu$m (2).

Field observations have offered evidence for the uptake of $HO_2$ by atmospheric aerosols (4, 5), which act as nucleating sites for cloud droplets. Furthermore, laboratory and theoretical studies in recent literature show that there is a particularly strong interaction between an $HO_2$ radical and a water molecule (6, 7). Calculated binding energies have been reported to be as much as 7.0 kcal/mol. The most recent of these has suggested that the binding of the complex is due to one hydrogen bond between the hydrogen of the radical and the oxygen of the water and a second weaker attraction between the terminal oxygen of the radical and one of hydrogens of the water (8). Such a configuration has a floppy five-membered ring-like structure and leaves the oxygen—oxygen bond of the complexed radical exposed for reaction. If the oxygen—oxygen bond is similarly exposed when an $HO_2$ radical is in the presence of multiple water molecules, there may be dramatic implications on our understanding of how the reactivity of $HO_2$ is affected by the presence of finite-sized water clusters and even macroscopic water droplets.

The focus of this theoretical work is to understand how the hydroperoxy radical behaves in the presence of multiple water molecules by studying the interactions between an $HO_2$ radical and an $(H_2O)_{20}$ spherical cage. The results are used to make general predictions about the behavior of $HO_2$ radicals in the presence of cloud droplets.

## Calculation Method

As a model of an $HO_2$ radical in the presence of a cloud droplet, we have examined $(H_2O)_{20}{\cdot}HO_2$ complexes. A 20-water system

*To whom correspondence may be addressed. E-mail: jfrancis@purdue.edu or kais@purdue.edu.



www.pnas.org/cgi/doi/10.1073/pnas.1733696100

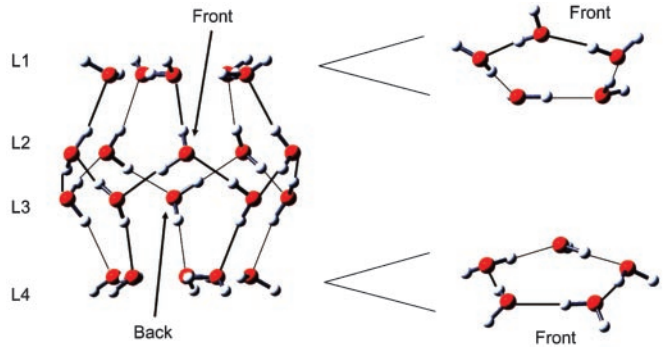


**Fig. 2.** Fully optimized structure of the $(H_2O)_{20}$ cage. This cluster has $S_{10}$ symmetry and can be viewed as being composed of four levels (L1–L4). (*Right*) For clarity, the diagram shows L1 and L4 tipped up and down, respectively.

was decided on after many preliminary calculations had been performed on smaller $(H_2O)_N{\cdot}HO_2$ clusters (where $N = 2$–6, 8, 10, 12, and 16). Although many hydrogen-bonding connectivities are possible for the $(H_2O)_{20}$ cluster (9–13), we selected a spherical cage-like structure with $S_{10}$ symmetry as its starting geometry. A water cage is ideally suited for these studies because it allows for the radical to be placed inside and hence surrounded by water molecules. Furthermore, selecting a cage with such a high degree of symmetry means that there will be a limited number of unique sites, both internal and external, to which the radical might bind, which significantly reduces the amount of computation time necessary for a thorough search. However, because of the number of heavy atoms involved, all the systematic searching that was used to locate minima of the potential energy surface was conducted by using unrestricted Hartree–Fock theory and a 6-31G(d) basis set. To determine whether this basis set would be sufficient for our purposes, optimizations were performed on the smaller $(H_2O)_N{\cdot}HO_2$ clusters with the 6-31G(d) and 6-31G(d,p) basis sets. The results of these two sets of optimizations were found to be in good agreement with each other. After the relevant minima were identified, both second-order Møller–Plesset perturbation theory single-point calculations and density functional theory optimizations were performed to check the effects of including electron–electron correlations.

Searches were conducted by placing the radical at many locations around the cage (including inside). At each location, multiple starting orientations were tried. In this article we report on two structures with the radical on the outside of the cage, $[(H_2O)_{20}{\cdot}HO_2]^{OUT}$, and one structure with the radical on the inside of the cage, $[(H_2O)_{20}{\cdot}HO_2]^{IN}$.

Once stationary points on the potential energy surface were identified, frequency analyses were carried out to verify that each structure reported was a minimum of the surface. After a structure had been established as a minimum, it was necessary to calculate, for comparison purposes, the binding energy between the radical and the water cluster. This was done by using the equation binding energy $= |E[(H_2O)_{20}{\cdot}HO_2] - E[(H_2O)_{20}] - E[HO_2]|$, where each bracketed structure was fully optimized in isolation. The GAUSSIAN 98 suite of programs (14) was used for all quantum calculations.

## Results

**$(H_2O)_{20}$ Spherical Cage.** The water cage can be thought of as a four-level structure, L1–L4, as is shown in Fig. 2. The top and bottom levels, L1 and L4, are cyclic pentamer rings in which each water molecule uses one of its hydrogens in a hydrogen bond within the ring and has its other hydrogen dangling. Because of this, all the hydrogens that bond L1 to L2 (and L3 to L4) are donated by L2 (and L3). The middle two levels, L2 and L3, also each consist of five water molecules. These are oriented such that each adjacent pair of water molecules on L2 (L3), along with a corresponding pair from L1 (L4) and one molecule from L3 (L2), form a pentamer ring on the side of the cluster. There are a total of 10 of these pentamer rings. All the water molecules from L2 and L3 have both of their hydrogens participating in hydrogen bonds; therefore the only dangling hydrogens are on L1 and L4. Thus, of the 40 hydrogen atoms, 30 participate in hydrogen bonding and 10 are dangling.

The first calculation performed was a full optimization (174 degrees of freedom) of this cage structure. If our only interest were in the $(H_2O)_{20}$ cage, such a difficult calculation would not be required, but because the presence of the radical will inevitably break the symmetry of the system, these full optimizations were absolutely necessary.

The absolute energy of the $(H_2O)_{20}$ cage, at the HF/6-31G(d) level of theory, was found to be −1,520.51273 a.u. with a binding energy per hydrogen bond of 6.2 kcal/mol. This is greater than the binding energy of the fully optimized water dimer (15), which is 5.6 kcal/mol [HF/6-31G(d)] and reveals that additional stability is brought to the cage via three-molecule (and higher) potential energy contributions.

**$[(H_2O)_{20}{\cdot}HO_2]^{OUT,SIDE}$.** For this configuration of the $(H_2O)_{20}{\cdot}HO_2$ complex, the hydrogen of the radical is hydrogen-bound to the oxygen of an L2-water molecule, and the terminal oxygen of the radical is hydrogen-bound to a dangling L1-hydrogen atom, where the above mentioned L1- and L2-water molecules are hydrogen-bound to each other. The central oxygen atom of the radical does not participate in hydrogen bonding for this structure. It can be seen from Fig. 3*a* that there is virtually no distortion of the cage shape except for a slight tug on the L1-hydrogen atom, which forms the hydrogen bond with the radical. The binding energy between the $(H_2O)_{20}$ and the radical was calculated to be 14.5 kcal/mol.

In Fig. 3*a Right*, we show an enlarged view of the $(H_2O)_2{\cdot}HO_2$ structure that is primarily responsible for the binding between the radical and the cage. The two dangling hydrogens of this structure are cis to each other. This is a somewhat destabilizing feature, and a single-point calculation reveals that this three-molecule structure is 1.8 kcal/mol less stable than the fully optimized $(H_2O)_2{\cdot}HO_2$, which has a binding energy of 13.3 kcal/mol. This 1.2 kcal/mol difference in binding energy between the $N = 2$ and $N = 20$ fully optimized structures is small and suggests that the binding of the radical to the cage, for this configuration, is a fairly localized phenomenon.

**$[(H_2O)_{20}{\cdot}HO_2]^{OUT,TOP}$.** As for the $[(H_2O)_{20}{\cdot}HO_2]^{OUT,SIDE}$ configuration, the $[(H_2O)_{20}{\cdot}HO_2]^{OUT,TOP}$ structure also has the radical bound to the outside of the cage via the hydrogen and terminal oxygen of the radical. This orientation for the radical is consistent with the results of our calculations performed on the smaller $(H_2O)_N{\cdot}HO_2$ clusters. The difference between the radical/cage bonding of the two $[(H_2O)_{20}{\cdot}HO_2]^{OUT}$ structures is that the radical of the $[(H_2O)_{20}{\cdot}HO_2]^{OUT,TOP}$ structure is bound to two adjacent L1-water molecules. The $[(H_2O)_{20}{\cdot}HO_2]^{OUT,TOP}$ structure is shown in Fig. 3*b*. To make this bonding configuration possible, the cage must undergo changes in its hydrogen-bonding connectivity. Because each L1-water molecule already accepts two foreign hydrogens for hydrogen bonding, structural changes in the cage are necessary to expose the oxygen atom of one of the L1-water molecules. The main changes involve the breaking of a hydrogen bond between an L1(L4)-oxygen atom and an L2(L3)-hydrogen atom, and the forming of a new hydrogen bond between the previously dangling hydrogen of the same L1(L4)-water molecule and the oxygen of the same L2(L3)-water molecule. To attain the binding configuration of this

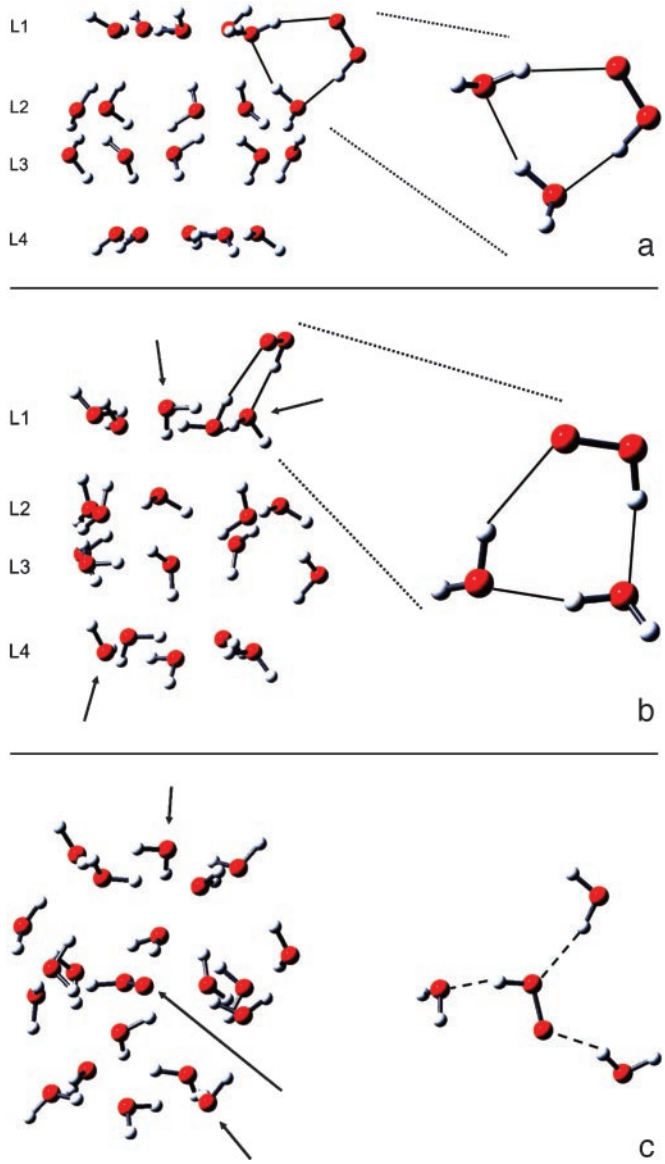


**Fig. 3.** Structures of the $(H_2O)_{20}{\cdot}HO_2$ $[(H_2O)_{20}{\cdot}HO_2]^{OUT,SIDE}$ (*a*), $[(H_2O)_{20}{\cdot}HO_2]^{OUT,TOP}$ (*b*), and $[(H_2O)_{20}{\cdot}HO_2]^{IN}$ (*c*) configurations. To the right of each cluster an expanded view of the relative orientation of the $HO_2$ radical and the water molecules to which it is hydrogen-bound is shown. (*a Right*) Both of the dangling hydrogens point out of the page. (*b Right*) The left dangling hydrogen points in, and the right dangling hydrogen points out.

$(H_2O)_{20}{\cdot}HO_2$ complex, the cage actually undergoes three occurrences of this structural change: two on L1 and one on L4. These sites are identified by arrows in Fig. 3*b*. The binding energy for this configuration is 22.7 kcal/mol. This is a full 8.2 kcal/mol more stable than the $[(H_2O)_{20}{\cdot}HO_2]^{OUT,SIDE}$ configuration of the previous section. The large excess of binding energy, in this case, is the result of the severe distortion and hydrogen-bonding connectivity rearrangement that the cage experiences.

The three-molecule cyclic structure that is primarily responsible for the bonding of this configuration has been enlarged and rotated and is shown in Fig. 3*b Right*. From this view, it can be seen that, for this three-molecule system, the two dangling hydrogens are trans to each other. This is a more stable configuration than the cyclic structure from Fig. 3*a*. In fact, this slightly contorted $(H_2O)_2{\cdot}HO_2$ structure is only 0.5 kcal/mol less stable than the fully optimized one.

**$[(H_2O)_{20}{\cdot}HO_2]^{IN}$.** The third configuration of $(H_2O)_{20}{\cdot}$ $HO_2$ that we are reporting has the radical inside the cage. Optimizations were started with various orientations for the radical, and the most stable optimized configuration is shown in Fig. 3*c*. Because none of the dangling hydrogens of the isolated cage are directed into the cage, some structural rearrangement was found to be necessary for any structures that have the radical inside. This particular configuration actually has three hydrogen bonds between the radical and the cage, where each of the atoms of the radical participate in one of the hydrogen bonds. The hydrogen of the radical can quite readily find a suitable hydrogen-bonding site because there are 10 oxygen atoms of water molecules (of L2 and L3; all 10 are equivalent) that have accepted only one foreign hydrogen. It is the oxygen atoms of the radical that require the structural rearrangement. When the radical is placed inside, two hydrogens, one from L2 and one from L3, bend inward to bond to the oxygen atoms of the radical. Then, to maintain the integrity of the cage, two nearby dangling hydrogens, one from L1 and the other from L4, bend down/up to replace the lost hydrogen bonds. The Fig. 3*c Right* shows the relative orientations of the radical and the three molecules to which it is hydrogen-bound. The binding energy for this configuration is 21.0 kcal/mol [HF/6-31G(d)]. This is only 1.7 kcal/mol less than the binding energy of the $[(H_2O)_{20}{\cdot}HO_2]^{OUT,TOP}$ configuration. Again, the large excess of binding energy results from distortion and hydrogen-bonding connectivity rearrangements.

The magnitude of electron–electron correlation was estimated by performing second-order Møller–Plesset perturbation theory single-point calculations on both the $[(H_2O)_{20}{\cdot}HO_2]^{OUT,TOP}$ and $[(H_2O)_{20}{\cdot}HO_2]^{IN}$ structures. The energy difference between these two structures, at the second-order Møller–Plesset perturbation/6-31G(d) level of theory, is 2.3 kcal/mol {where again the $[(H_2O)_{20}{\cdot}HO_2]^{OUT,TOP}$ structure is energetically preferred}. The $[(H_2O)_{20}{\cdot}HO_2]^{OUT,TOP}$ and $[(H_2O)_{20}{\cdot}HO_2]^{IN}$ structures were then reoptimized at the density functional/6-31G(d) level of theory. These calculations predicted a 3.8 kcal/mol energy difference between the two configurations.

**Potential Energy Curves for the Approach of the $HO_2$ Radical.** After the $(H_2O)_{20}{\cdot}HO_2$ structures were found, potential energy curves for each were established to obtain a clearer picture of the energetics of the system as the radical approaches the cluster. The curves were calculated, in each case, by starting with the fully optimized structure (the minimum of each curve) and placing the radical in different positions along a line connecting the central oxygen atom of the radical and the closest oxygen atom of the cage. During this motion, the relative (angular) orientation of the radical and the cage was maintained. The radical was moved incrementally both closer to and farther from the cage. At each distance, a single point energy was measured. These data are plotted in Fig. 4.

Although the three curves have different energy values, there are two common features among them: the distances at the minima ($R_{min}$) and the distances at which the interaction energies approach zero ($R_{E\to 0}$). From the plots it can be seen that $R_{min}$ = 2.75, 2.78, and 2.68 Å for the $[(H_2O)_{20}{\cdot}HO_2]^{OUT,SIDE}$, $[(H_2O)_{20}{\cdot}HO_2]^{OUT,TOP}$, and $[(H_2O)_{20}{\cdot}HO_2]^{IN}$ structures, respectively, and that $R_{E\to 0} \approx 5$ Å for both of the $[(H_2O)_{20}{\cdot}HO_2]^{OUT}$ structures. The fact that these numbers have small differences suggests that the shortest oxygen—oxygen distance is the dominant factor for predicting the energetics between the radical and the water cluster.

The presence of the $[(H_2O)_{20}{\cdot}HO_2]^{OUT}$ potential energy wells suggests that $HO_2$ radicals will be attracted to the surfaces of water droplets, and the depth of the $[(H_2O)_{20}{\cdot}HO_2]^{OUT,TOP}$ well, in particular, suggests that the $HO_2$ radical will become incorporated with the water-droplet surface. Furthermore, the depth of the $[(H_2O)_{20}{\cdot}HO_2]^{IN}$ well implies that it is quite possible for

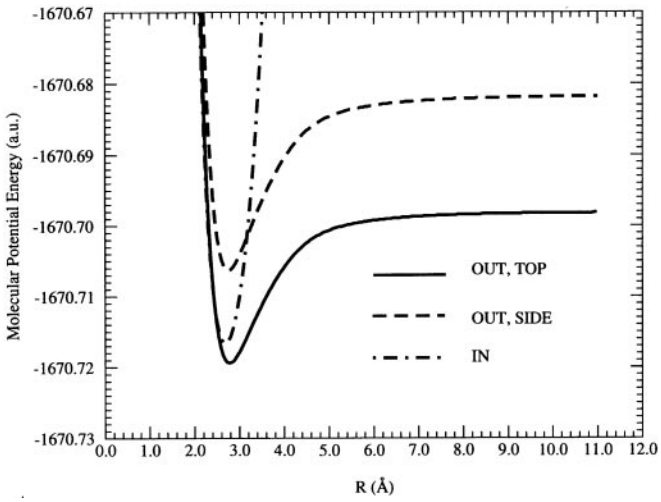


**Fig. 4.** Molecular potential energy curves for each of the $(H_2O)_{20}{\cdot}HO_2$ configurations plotted as functions of the distance (*R*) between the central oxygen atom of the radical and the closest oxygen atom of a cage water molecule.

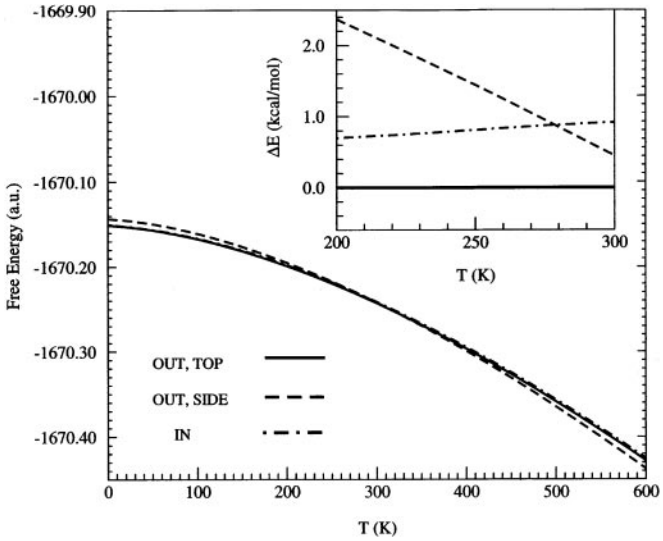


**Fig. 5.** Energies, including thermal free-energy contributions, for the three $(H_2O)_{20}{\cdot}HO_2$ configurations plotted as functions of temperature (K). (*Inset*) Shown, within the atmospheric temperature range, are the energy differences between the curves, where the energy of $[(H_2O)_{20}{\cdot}HO_2]^{OUT,TOP}$ is taken as the reference energy at each temperature.

the radical to enter the cage; the droplet-scale analogy for this phenomenon would be the dissolving of the radical.

## Discussion and Implications for the Interactions of $HO_2$ and Water Surfaces

As a model of an $HO_2$ radical in the presence of a cloud droplet, we studied the energetics of an $(H_2O)_{20}{\cdot}HO_2$ cluster where the $(H_2O)_{20}$ was initialized as a spherical cage with $S_{10}$ symmetry. Three configurations of $(H_2O)_{20}{\cdot}HO_2$ are reported here: two of which have the radical on the outside of the cage and one of which has the radical contained within the cage.

Of the three structures reported, the first one, $[(H_2O)_{20}{\cdot}HO_2]^{OUT,SIDE}$, has the weakest binding energy at 14.5 kcal/mol and suffers almost no cage distortion. The second configuration reported, $[(H_2O)_{20}{\cdot}HO_2]^{OUT,TOP}$, is the most strongly bound configuration with a binding energy of 22.7 kcal/mol. It undergoes a significant degree of distortion during optimization. For both of the $[(H_2O)_{20}{\cdot}HO_2]^{OUT}$ configurations, the cage/radical bonding was between the hydrogen and terminal oxygen of the radical and the two of the cage water molecules.

A significant difference between the two $[(H_2O)_{20}{\cdot}HO_2]^{OUT}$ structures is that during optimization, the $[(H_2O)_{20}{\cdot}HO_2]^{OUT,TOP}$ configuration undergoes rearrangement of its hydrogen-bonding topology and becomes distorted. For this reason, the $[(H_2O)_{20}{\cdot}HO_2]^{OUT,TOP}$ case provides a better picture of a liquid-phase cloud droplet. This is because liquid-phase water molecules can rearrange themselves to accommodate an adsorbed gas-phase species. The $[(H_2O)_{20}{\cdot}HO_2]^{OUT,SIDE}$ configuration, which underwent very little distortion, better approximates a gas-phase chemical species on a solid-phase ice surface, because the water molecules of ice are fixed in position and orientation and therefore cannot reorient themselves (to the same degree) to accommodate the gas-phase species. This suggests that a gas-phase chemical species will bind more strongly to liquid water than to ice because of the possibility of molecular rearrangement at the surface.

The third configuration reported $[(H_2O)_{20}{\cdot}HO_2]^{IN}$ actually has the radical inside the cage. In this case, the cage also undergoes significant distortion, which again leads to a larger binding energy between the radical and the cage. The binding energy for $[(H_2O)_{20}{\cdot}HO_2]^{IN}$ is 21.0 kcal/mol, which is only 1.7 kcal/mol smaller than the binding energy of the $[(H_2O)_{20}{\cdot}HO_2]^{OUT,TOP}$ configuration. This difference was found to be somewhat larger when electron–electron correlation was included. The fact that the $[(H_2O)_{20}{\cdot}HO_2]^{OUT,TOP}$ configuration is more stable than $[(H_2O)_{20}{\cdot}HO_2]^{IN}$ implies that, energetically, the radical prefers to be on the outside of the cage even though the internal configuration has three hydrogen bonds between the radical and the cage. The magnitude of this difference, however, suggests that there may be a partitioning of $HO_2$ radicals between the external and internal states: $[(H_2O)_{20}{\cdot}HO_2]^{OUT} \leftrightarrow [(H_2O)_{20}{\cdot}HO_2]^{IN}$. The extent of such a partition would be a function of several factors including temperature, pressure, and the concentration of the radical. The values of these quantities can vary widely for different regions of the atmosphere.

The idea of a partitioning of $HO_2$ radicals between the surface and the bulk enhances our current understanding of how atmospheric radical species interact with cloud droplets. A partitioning implies that $HO_2$ radical chemistry can occur on the surface of a cloud droplet and within the bulk of the same droplet simultaneously.

Potential energy curves were then created for each of the $(H_2O)_{20}{\cdot}HO_2$ configurations. Although they have quite different energy values at their minima, the three curves do have in common both the distances at their minima and the distances {for the two $[(H_2O)_{20}{\cdot}HO_2]^{OUT}$ configurations} at which the interaction energy approaches zero. This suggests that the dominant feature for predicting the energetics between $HO_2$ and the $(H_2O)_{20}$ cage is the distance between the central oxygen atom of the radical and the closest oxygen atom of a cage water molecule.

A final set of calculations was performed to determine how the relative energies of the $(H_2O)_{20}{\cdot}HO_2$ complexes would change with variations in temperature. Free energies were calculated for each of the $(H_2O)_{20}{\cdot}HO_2$ structures as functions of temperature between 0 and 600 K. As can be seen in Fig. 5, these energies all decrease (become more negative) with increasing temperature. It can be seen from Fig. 5 *Inset* that within the atmospheric temperature range, 200–300 K, the $[(H_2O)_{20}{\cdot}HO_2]^{OUT,\ SIDE}$ and $[(H_2O)_{20}{\cdot}HO_2]^{IN}$ curves cross at 280 K and that the $[(H_2O)_{20}{\cdot}HO_2]^{OUT,TOP}$ curve is always the most stable configuration. The shrinking of the energy gap, as the atmospherically relevant temperature range is approached, however, supplies

further evidence for the idea of a partitioning between states that was described above.

Laboratory studies have demonstrated that the uptake of gas-phase $HO_2$ is limited only by its rate of diffusion to a water surface (16), which means that the mass accommodation, the fraction of particles striking a liquid surface that will penetrate the surface and become incorporated into the bulk, approaches unity. Heterogeneous $HO_2$ loss constitutes 5–10% of the homogeneous gas-phase chemical loss for low to moderate aerosol-loading conditions and becomes comparable to gas-phase chemical loss for high aerosol loading (17, 18). These estimates assume that $HO_2$ is irreversibly destroyed after being accommodated by the aerosol surface, and this assumption remains the principle uncertainty in the process. The present results suggest that this assumption may not be a valid one. The question of whether subsequent $HO_2$ chemistry occurs on the surface or in the bulk requires further study; however, results of this study suggest that $HO_2$ chemistry may be occurring on the aerosol surface or between surface-bound and gas-phase reactants. Furthermore, the idea of water-soluble radicals suggests that the interiors of cloud droplets may be an additional medium in which atmospheric radical chemistry may occur.

## Conclusions

We have presented here a theoretical study performed to examine the interactions of an $HO_2$ radical with a model water surface. We have found that the energy difference between a radical on a surface and one surrounded by water molecules can be small. Calculated free-energy curves were used to confirm that this behavior will be preserved at the finite temperatures of the atmosphere. The small energy difference between the internal and external configurations was used to argue that a partitioning between surface-bound and dissolved radicals may occur. Such a partitioning implies that radical chemistry may occur on the surface of a cloud droplet and within the cloud droplet simultaneously. This idea of the partitioning between surface-bound and dissolved $HO_2$ radicals is significant because of the roles that $HO_2$ plays in the budgeting of the chemical species of the atmosphere. For example, it is known that $HO_2$ radicals can be converted to hydrogen peroxide with copper-containing aerosols as the medium. The mechanism proposed is (ref. 19 and references therein)

$$HO_{2(aq)} + Cu^{2+} \rightarrow H_3O^+ + Cu^+$$

$$HO_2 + Cu^+ \rightarrow HO_2^- + Cu^{2+}$$

$$HO_2^- + H_3O^+ \rightarrow H_2O_2 + H_2O.$$

The rate of production of $H_2O_2$ is proportional to the aqueous-phase abundances of both Cu and $HO_2$ in solution. The rate of production of $H_2O_2$ by this mechanism most certainly will be impacted by the reduced fraction of $HO_2$ in the bulk. If the production rate for $H_2O_2$ from this reaction is used as a measure of the concentration of $HO_2$, the present work suggests that the result may be artificially low, because all of the $HO_2$ will not be fully solvated. Further studies involving molecular dynamics simulations looking at $HO_2$ in water along with Cu ions should provide insight into how the $H_2O_2$ production rate will be impacted by $HO_2$ radicals bound to water surfaces.

We acknowledge the financial support of National Science Foundation Grant NSF-0136453-CHE.

1. Finlayson-Pitts, B. J. & Pitts, J. N., Jr. (2000) in *Chemistry of the Upper and Lower Atmosphere: Theory, Experiments, and Applications* (Academic, San Diego).
2. Hanson, D. R., Ravishankara, A. R. & Solomon, S. (1994) *J. Geophys. Res.* **99,** 3615–3629.
3. Gertner, B. J. & Hynes, J. T. (1996) *Science* **271,** 1563–1566.
4. Mauldin, R. L., III, Frost, G. J., Chen, G., Tanner, D. J., Prevot, A. S. H., Davis, D. D. & Eisele, F. L. (1998) *J. Geophys. Res.* **103,** 16713–16729.
5. Saylor, R. D. (1997) *Atmos. Environ.* **31,** 3653–3658.
6. Sander, S. P. & Peterson, M. E. (1984) *J. Phys. Chem.* **88,** 1566–1571.
7. Aloisio, S., Francisco, J. S. & Friedl, R. R. (2000) *J. Phys. Chem. A* **104,** 6597–6601.
8. Aloisio, S. & Francisco, J. S. (1998) *J. Phys. Chem. A* **102,** 1899–1902.
9. Cioslowski, J. & Nanayakkara, A. (1992) *Int. J. Mod. Phys. B* **6** (23 and 24), 3687–3693.
10. Maheshwary, S., Patel, N., Sathyamurthy, N., Kulkarni, A. D. & Gadre, S. R. (2001) *J. Phys. Chem. A* **105,** 10525–10537.
11. Chiu, Y. & Wang, B. (1993) *J. Mol. Struct.* **283,** 13–25.
12. Tsai, C. J. & Jordan, K. D. (1993) *J. Phys. Chem.* **97,** 5208–5210.
13. Wales, D. J. & Hodges, M. P. (1998) *Chem. Phys. Lett.* **286,** 65–72.
14. Frisch, M. J., Trucks, G. W., Schlegel, H. B., Scuseria, G. E., Robb, M. A., Cheeseman, J. R., Zakrzewski, V. G., Montgomery, J. A., Jr., Stratmann, R. E. & Burant, J. C. (1998) GAUSSIAN 98 (Gaussian, Pittsburgh), Revision A.7.
15. Kim, K. & Jordan, K. D. (1994) *J. Phys. Chem.* **98,** 10089–10094.
16. Hanson, D. R., Burkholder, J. B., Howard, C. J. & Ravishankara, A. R. (1992) *J. Phys. Chem.* **96,** 4979–4985.
17. Cantrell, C. A., Shetter, R. E., Gilpin, T. M. & Calvert, J. G. (1996) *J. Geophys. Res.* **101,** 14643–14652.
18. Kanaya, Y., Sadanaga, Y., Matsumoto, J., Sharma, U. K., Hirokawa, J., Kajii, Y. & Akimoto, H. (2000) *J. Geophys. Res.* **105,** 24205–24222.
19. Jacob, D. J. (1999) *Atmos. Environ.* **34,** 2131–2159.